LIFETIME MEASUREMENTS USING RDDS METHOD IN THE VICINITY OF ^{78}Ni[*]

C. Delafosse, D. Verney, A. Gottardo, F. Ibrahim
S. Franchoo, I. Matea, L. Olivier, C. Portail

Institut de Physique Nucléaire, CNRS-IN2P3, Univ. Paris-Sud
Université Paris-Saclay, 91406 Orsay Cedex, France

E. Clément, A. Lemasson, C. Michelagnoli
M. Babo, B. Jacquot

Grand Accélérateur National d'Ions Lourds (GANIL)
CEA/DSM-CNRS/IN2P3, Caen, France

A. Goasduff, D.R. Napoli

Instituto Nazionale di Fisica Nucleare, Laboratori Nazionali di Legnaro
35020 Legnaro, Italy

J. Ljungvall, A. Korichi, G. Georgiev, T. Konstantinopoulos

CSNSM, CNRS-IN2P3, Univ. Paris-Sud, Université Paris-Saclay, 91406 Orsay, France

S.M. Lenzi, A. Boso, D. Mengoni, F. Recchia

Departamento di Fisica e Astronomia, Universita di Padova and
INFN, Sezione di Padova, 35131 Padova, Italy

C. Andreoiu

Dept. of Chemistry, Simon Fraster University, Burnaby, BC, V5A S16, Canada

F. Didierjean

Institut Pluridisciplinaire Hubert Curien, CNRS-IN2P3-Université de Strasbourg
67037 Strasbourg, France

J. Dudouet, G. Maquart, N. Redon, O. Stezowski

Univ. Lyon, Université Lyon 1, CNRS/IN2P3, IPN-Lyon, 69622, Villeurbanne, France

A. Gadea, R.M. Pérez-Vidal

IFIC, CSIC-Univ. Valencia, Apartado Oficial 22085, 46071 Valencia, Spain

M. Zielińska

CEA de Saclay, IRFU, 91191 Gif-sur-Yvette, France

Reduced quadrupole transition probabilities for low-lying transitions in neutron-rich $N = 52$ isotones ^{88}Kr and ^{86}Se were investigated with a recoil distance Doppler shift (RDDS) experiment. The experiment was performed at GANIL (Caen, France) using the Orsay Universal Plunger System (OUPS) for the RDDS technique and the AGATA array for the γ-ray detection coupled to the VAMOS++ magnetic spectrometer for an event-by-event particle identification. In ^{88}Kr, the lifetimes of seven levels were determined and in ^{86}Se, the lifetimes of five levels were determined. The deduced $B(\text{E2}; 2_1^+ \rightarrow 0_1^+)$ are compared with mean-field and shell-model calculations.

1. Introduction

The neutron-rich Zr, Sr, Kr, and Se isotopes with neutron numbers $N = 50$–60 continue to attract attention for their display of rapid changes in the evolution of collectivity and the mounting evidence for shape coexistence towards $Z = 28$ [1]. Since the first indications from the trends in the first 2^+ energies in Zr [2] and Sr [3] decades ago, studies of transition strengths and moments have most recently cemented a picture of a sudden increase in collectivity and shape changes for Sr [4], and a quantum phase transition in the shape of the Zr isotopes [5] at $N = 60$. In the Kr isotopic chain, just four and two protons below Zr and Sr, respectively, a rather gradual onset of collectivity towards $N = 60$ was concluded from mass measurements [6], Coulomb excitation [7], and fast-timing measurements [8], placing the $N = 60$ isotone ^{96}Kr at the low-Z boundary of the region of deformation described above [9]. Present information on the Se and Kr chain is limited to excitation energies out to ^{94}Se [10], the $B(\text{E2}\uparrow)$ strength of ^{86,88}Kr and ^{86}Se from Coulomb excitation [11], and lifetimes of excited states measured for ^{84,86}Se [12]. The present work extends the investigation of the quadrupole properties of nuclei in this mass region towards the doubly magic $Z = 28$, $N = 50$ shell closures. We report the measurements of several states lifetimes of excited states in ^{88}Kr and ^{86}Se ($N = 52$) with improved accuracy as compared to the literature and we obtained, for the first time, absolute lifetimes measurements for higher energy Yrast and near-Yrast states in ^{88}Kr and ^{86}Se. The results are compared to shell model calculations in the $\pi(fpg)$–$\nu(sdgh)$ shell relative to a ^{78}Ni core and to HFB-5DCH mean-field calculation.

2. Experiment

The experiment was performed at GANIL. The ^{88}Kr and ^{86}Se nuclei were produced by fusion–fission and transfer–fission of a ^{238}U beam at 6.2 AMeV on a Be target with a thickness of 2.07 mg/cm^2. The average intensity of the beam was 0.25 pnA. The fission fragments were identified and their velocities were determined with the magnetic spectrometer VAMOS++ [13] located at 28° from the beam direction in order to select the neutron-rich Ge region. The identification of fission products was based on the ion trajectory reconstruction using: *(i)* the x and y entrance coordinates on the target multiwire chambers (TMW) [14], *(ii)* the x and y coordinates in the drift chambers (DC) locate at the focal plane, *(iii)* the time of flight (ToF) of the fission products between the TMW and the array of parallel plates of the multiwire chambers (MWPPAC) located at the focal plane, *(iv)* the partial (ΔE) and total (E) energies released in the 20 sections of the ionization chambers (IC). The selection of the atomic number (Z) was made using ΔE *versus* E correlation data. The isotope selection was made in three steps. First, the ratio $\frac{A}{Q}$ was reconstructed using the magnetic rigidity and the ToF. Then, the ion charge was identified through an evaluation of the mass obtained from the measurement of the kinetic energy divided by $\frac{A}{Q}$. The charge states Q are selected in the bi-dimensional matrix Q_E *versus* $\frac{A}{Q}$. Finally, for each charge state Q, the mass distribution was obtained using the selection of VAMOS events of a given mass A (Fig. 1).
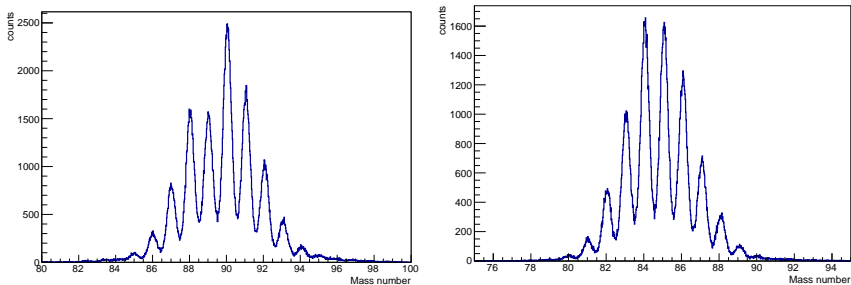

Fig. 1. Mass distribution of Kr (left) and Se (right) isotopes obtained with VAMOS++.

The prompt γ-rays were detected by the AGATA detector [15]. The setup comprised eight triple cluster modules placed at 18.6 cm from the target and at backward angles. Using the grid search algorithm for pulse shape analysis (PSA) [16], the γ-ray interaction points were located in the Ge material with a resolution (FWHM) of about 5 mm at 1 MeV [17]. The energies of γ rays were obtained by applying offline the OFT γ-ray tracking algorithm [18]. The γ-rays spectrum of the nuclei of interest was Doppler

corrected event-by-event using the velocity vector measured in VAMOS and the position of the first interaction in AGATA. Lifetime measurements were performed using the Recoil Distance Doppler Shift (RDDS) technique using the OUPS plunger [19]. An Mg degrader foil with a thickness of 5 mg/cm^2 was placed downstream from the target in order to slow down the fission-products. Depending on the lifetime of the state of interest and the distance between target and degrader, γ-ray emission happened partially before and after the degrader at respective recoil velocities β_{before} and β_{after}. Consequently, for each transition, two components (one shifted and one unshifted) were observed in the γ-ray spectrum. As β_{after} is precisely calculated from VAMOS information, the "after" component is accurately Doppler corrected (unshifted peak), whereas the "before" component is shifted to lower energy (AGATA being placed at backward angles). Lifetimes are deduced from the ratio of intensity of the two components. The degrader was placed at three distances from the target: 120(10) μm, 270(10) μm and 520(10) μm with a measuring time of 75 h, 75 h and 85 h, respectively. The spectrum containing the sum of statistics collected at all target–degrader distances for ^{86}Se is shown in Fig. 2.
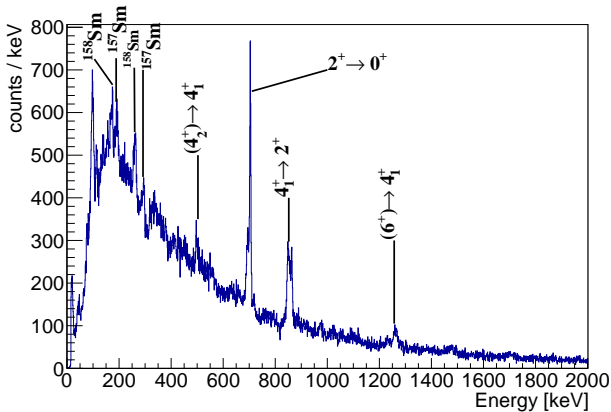

Fig. 2. γ-spectrum in AGATA in coincidence with ^{86}Se identified in VAMOS.

3. Lifetime results

The lifetime extraction procedure is described in Refs. [12, 20]. We measured the ratio $R = \frac{I_{\text{U}}}{I_{\text{U}}+I_{\text{S}}}$ (I_{U} and I_{S} are the integral of the unshifted and shifted components of the peak, respectively) for all the distances (when statistics allows). In the case of low statistics, this ratio was obtained from a sum spectrum including measurement at all distances. The velocity of the residue measured in VAMOS was β_{after} from which β_{before} is deduced using the LISE++ software, see Table I. The times of flight between target and

degrader for the distances are then respectively obtained using $t = \frac{dc}{\beta_{\text{before}}}$ where d is the target–degrader distance and c the speed of light. Seven transitions were attributed to ^{88}Kr: 440, 460, 609, 753, 775, 868, 1517 and 1523 keV [21], and five were attributed to ^{86}Se: 504, 704, 864, 991 and 1279 keV [22], giving the level scheme shown in Fig. 3 (left) and Fig. 3 (right), respectively. Lifetimes were extracted by fitting the $R(t)$ data points with the corresponding Bateman equation (see Fig. 4 and 5).
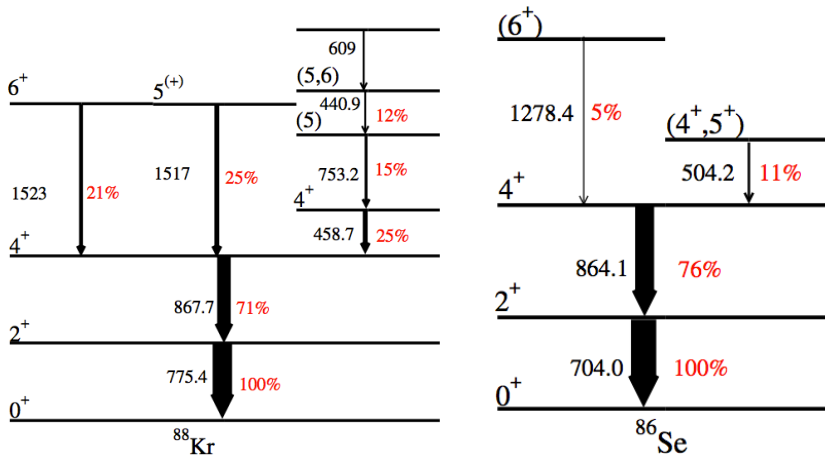

Fig. 3. (Colour on-line) Observed level scheme of ^{88}Kr (left) and ^{86}Se (right). In red/grey are indicated the observed relative γ-intensities in this work.
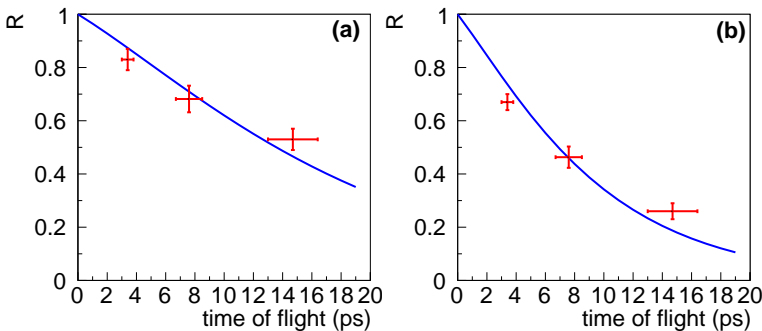

Fig. 4. Fit of the R ratio as a function of time of flight between target and degrader using the Bateman equations for the 2^+ (a) and 4_1^+ (b) states of ^{88}Kr.

When the lifetime is too short, only data from the shortest distance measurement can be exploited. In this case, we use the technique used in Ref. [20]. It was used, for example, to determined the lifetimes of the higher energy states in ^{88}Kr. All the lifetimes obtained are reported in Table I.
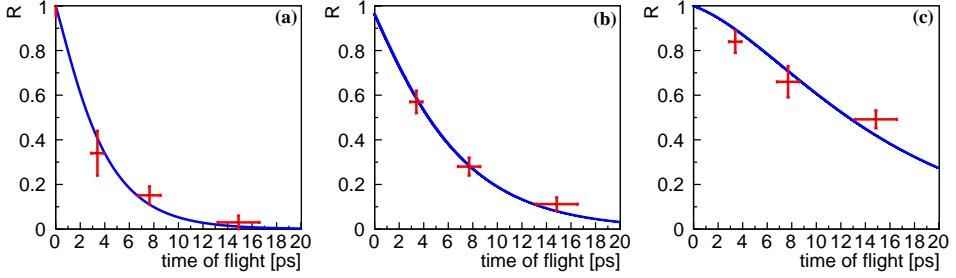
Fig. 5. The same as Fig. 4 but for (4_2^+) state (a), 4_1^+ state (b) and 2^+ state (c) of ^{86}Se.

TABLE I

Summary of the experimental lifetimes obtained in ^{88}Kr and ^{86}Se (the ones with a star are effective lifetimes *i.e.* uncorrected from feeding lifetimes). The corresponding B(E2) and B(M1) values are also reported.

^{A}X	β_{before}	$J^{\pi i} \to J^{\pi f}$	E_γ [keV]	τ [ps]	B(E2 $\downarrow$) [e^2 fm^4]	B(M1 $\downarrow$) [μ_N^2]
^{88}Kr	0.118(13)	$2^+ \to 0^+$	775.4(1)	$10.6^{+4.8}_{-5.0}$	274^{+244}_{-85}	—
		$4_1^+ \to 2^+$	867.7(1)	$6.6^{+2.6}_{-2.3}$	250^{+71}_{-134}	—
		$(4_2^+) \to 4_1^+$	458.7(6)	$4.3^{+2.6}_{-2.0}$	—	$0.14^{+0.12}_{-0.05}$
		$(6^+) \to 4_1^+$	1523.0(6)	$6.4^{+2.0}_{-3.5}(*)$	$15.5^{+18.7}_{-3.7}$	—
		$(5) \to 4_1^+$	1515.3(10)	$3.2^{+1.0}_{-0.5}$ (*)	$31.8^{+5.9}_{-7.6}$	—
		$(5) \to 4_2^+$	753.2(8)	$0.9^{+1.3}_{-0.1}$	—	$0.15^{+0.02}_{-0.09}$
		$(6^+) \to (5)$	440.9(8)	$1.7^{+0.4}_{-0.5}(*)$	—	$0.39^{+0.16}_{-0.07}$
^{86}Se	0.116(13)	$2^+ \to 0^+$	704.0(1)	$10.3^{+1.2}_{-2.2}$	456^{+124}_{-48}	—
		$4_1^+ \to 2^+$	864.1(3)	$5.5^{+0.9}_{-0.9}$	306^{+61}_{-42}	—
		$(4_2^+) \to 4_1^+$	504.2(5)	$3.2^{+0.6}_{-0.8}$ (*)	—	$0.13^{+0.05}_{-0.01}$
		$(6^+) \to 4_1^+$	1279.3(9)	$2.7^{+1.2}_{-0.9}$ (*)	88^{+44}_{-17}	—
		$(5^+) \to (4_2^+)$	990.7(9)	$1.1^{+0.5}_{-1.1}$ (*)	—	≤ 0.03

4. Conclusion

In this work, we report the lifetime measurements of Yrast and near-Yrast states in $N = 52$ isotones ^{88}Kr and ^{86}Se (see Table I). The obtained lifetimes of the first excited 2_1^+ states are compatible with both Coulomb excitation and previous RDDS measurements and with both shell-model using an inert core of ^{78}Ni [23] and beyond mean-field calculations [24] (Table II).

Comparison of $B(E2)$ values obtained in this work with available measurements in the literature and shell model (SM:Ni78-II) [23] and mean-field calculations (HFB-5DCH) [24].

^AX	$J^{\pi i} \to J^{\pi f}$	This work	Exp. literature	SM:Ni78-II	HFB-5DCH
			$B(E2\downarrow)$ [e^2 fm^4]		
^{88}Kr	$2^+ \to 0^+$	274^{+244}_{-85}	$262(38)$ [11]	371	389
^{86}Se	$2^+ \to 0^+$	456^{+124}_{-48}	438^{+259}_{-171} [12]/$422(64)$ [11]	436	447
^{86}Se	$4^+_1 \to 2^+$	306^{+61}_{-42}	≥ 140 [12]	329	—

REFERENCES

[1] C. Delafosse *et al.*, *Phys. Rev. Lett.* **121**, 192502 (2018).

[2] E. Cheifetz *et al.*, *Phys. Rev. Lett.* **25**, 38 (1970).

[3] H. Wollnik *et al.*, *Nucl. Phys. A* **291**, 355 (1977).

[4] J.-M. Régis *et al.*, *Phys. Rev. C* **95**, 054319 (2017).

[5] T. Togashi *et al.*, *Phys. Rev. Lett.* **117**, 172502 (2016).

[6] S. Naimi *et al.*, *Phys. Rev. Lett.* **105**, 032502 (Jul 2010).

[7] M. Albers *et al.*, *Phys. Rev. Lett.* **108**, 062701 (2012).

[8] J.-M. Régis *et al.*, *Phys. Rev. C* **90**, 067301 (2014).

[9] J. Dudouet *et al.*, *Phys. Rev. Lett.* **118**, 162501 (2017).

[10] I.N. Gratchev *et al.*, *Phys. Rev. C* **95**, 051302 (2017).

[11] B. Elman *et al.*, *Phys. Rev. C* **96**, 044332 (2017).

[12] J. Litzinger *et al.*, *Phys. Rev. C* **92**, 064322 (2015).

[13] M. Rejmund *et al.*, *Nucl. Instrum. Methods Phys. Res. A* **646**, 184 (2011).

[14] M. Vandebrouck *et al.*, *Nucl. Instrum. Methods Phys. Res. A* **812**, 112 (2016).

[15] S. Akkoyun *et al.*, *Nucl. Instrum. Methods Phys. Res. A* **668**, 26 (2012).

[16] R. Venturelli, D. Bazzacco, Adaptive Grid Search as Pulse Shape Analysis Algorithm for γ-Tracking and Results, LNL Annual Report 2004, 2005.

[17] B. Bruyneel, B. Birkenbach, P. Reiter, *Eur. Phys. J. A* **52**, 70 (2016).

[18] A. Lopez-Martens *et al.*, *Nucl. Instrum. Methods Phys. Res. A* **533**, 454 (2004).

[19] J. Ljungvall *et al.*, *Nucl. Instrum. Methods Phys. Res. A* **679**, 61 (2012).

[20] F. Didierjean *et al.*, *Phys. Rev. C* **96**, 044320 (2017).

[21] A. Astier *et al.*, *Phys. Rev. C* **88**, 024321 (2013).

[22] F. Drouet *et al.*, *EPJ Web Conf.* **62**, 01005 (2013).

[23] K. Sieja, private communication.

[24] J.P. Delaroche *et al.*, *Phys. Rev. C* **81**, 014303 (2010).